


# Simulation of circularly polarized luminescence spectra using coupled cluster theory

Cite as: J. Chem. Phys. **142**, 154101 (2015); <https://doi.org/10.1063/1.4917521>

Submitted: 17 February 2015 . Accepted: 02 April 2015 . Published Online: 15 April 2015

Harley R. McAlexander, and T. Daniel Crawford 



View Online



Export Citation



CrossMark

## ARTICLES YOU MAY BE INTERESTED IN

[A solid-state dedicated circularly polarized luminescence spectrophotometer: Development and application](#)

Review of Scientific Instruments **87**, 075102 (2016); <https://doi.org/10.1063/1.4954725>

[General theory of circularly polarized emission and magnetic circularly polarized emission from molecular systems](#)

The Journal of Chemical Physics **65**, 1011 (1976); <https://doi.org/10.1063/1.433177>

[Chiroptical properties from time-dependent density functional theory. I. Circular dichroism spectra of organic molecules](#)

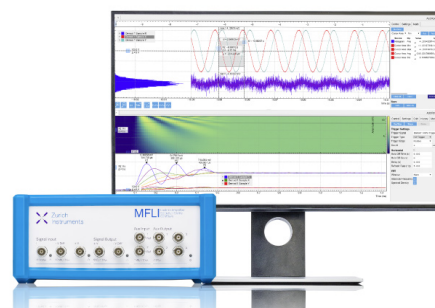
The Journal of Chemical Physics **116**, 6930 (2002); <https://doi.org/10.1063/1.1436466>

## Challenge us.

What are your needs for periodic signal detection?



Zurich  
Instruments



# Simulation of circularly polarized luminescence spectra using coupled cluster theory

Harley R. McAlexander and T. Daniel Crawford<sup>a)</sup>

Department of Chemistry, Virginia Tech, Blacksburg, Virginia 24061, USA

(Received 17 February 2015; accepted 2 April 2015; published online 15 April 2015)

We report the first computations of circularly polarized luminescence (CPL) rotatory strengths at the equation-of-motion coupled cluster singles and doubles (EOM-CCSD) level of theory. Using a test set of eight chiral ketones, we compare both dipole and rotatory strengths for absorption (electronic circular dichroism) and emission to the results from time-dependent density-functional theory (TD-DFT) and available experimental data for both valence and Rydberg transitions. For two of the compounds, we obtained optimized geometries of the lowest several excited states using both EOM-CCSD and TD-DFT and determined that structures and EOM-CCSD transition properties obtained with each structure were sufficiently similar that TD-DFT optimizations were acceptable for the remaining test cases. Agreement between EOM-CCSD and the Becke three-parameter exchange function and Lee-Yang-Parr correlation functional (B3LYP) corrected using the Coulomb attenuating method (CAM-B3LYP) is typically good for most of the transitions, though agreement with the uncorrected B3LYP functional is significantly worse for all reported properties. The choice of length vs. velocity representation of the electric dipole operator has little impact on the EOM-CCSD transition strengths for nearly all of the states we examined. For a pair of closely related  $\beta,\gamma$ -enones, (1*R*)-7-methylenebicyclo[2.2.1]heptan-2-one and (1*S*)-2-methylenebicyclo[2.2.1]heptan-7-one, we find that EOM-CCSD and CAM-B3LYP agree with the energetic ordering of the two possible excited-state conformations, resulting in good agreement with experimental rotatory strengths in both absorption and emission, whereas B3LYP yields a qualitatively incorrect result for the CPL signal of (1*S*)-2-methylenebicyclo[2.2.1]heptan-7-one. Finally, we predict that one of the compounds considered here, *trans*-bicyclo[3.3.0]octane-3,7-dione, is unique in that it exhibits an achiral ground state and a chiral first excited state, leading to a strong CPL signal but a weak circular dichroism signal. © 2015 AIP Publishing LLC. [<http://dx.doi.org/10.1063/1.4917521>]

## I. INTRODUCTION

A variety of spectroscopic techniques are widely employed to assist in the determination of the absolute stereochemical configurations of chiral compounds<sup>1-5</sup>—the important class of molecules lacking an improper rotation axis—that take advantage of the difference in the indices of refraction (birefringence), absorption (dichroism), or scattering (Raman optical activity) between left- and right-circularly polarized light when interacting with a non-racemic sample. The emission counterpart to electronic circular dichroism (ECD) is circularly polarized luminescence (CPL); the former provides structural information about the ground state, and the latter accesses complementary characteristics of the excited state. When only minor changes in the geometry occur between the ground state and excited state, CPL and ECD spectra will exhibit transitions similar in magnitude and sign, but alterations in the geometry can lead to significant differences between the two—sometimes even changes in sign of certain rotational strengths.

Over the last several decades, measurements of CPL spectra have found a home in studies of proteins,<sup>6,7</sup> transition metal complexes,<sup>8</sup> and even polymers.<sup>9</sup> CPL also opens the

door for novel chiroptical experiments, such as those probing achiral luminescent materials in chiral environments<sup>10,11</sup> and exciting chiral solutions with only right- or left-hand circularly polarized light and monitoring the emission.<sup>12-14</sup> Indeed, it has also been shown that certain fireflies that have a right and left lantern also exhibit CPL.<sup>15</sup> Recent advances in instrumentation such as the development of light-emitting diode sources promise to increase the practicality and usage of CPL measurements.<sup>16</sup>

The investigation of absolute configuration *via* CPL—like its circular dichroism, birefringence, and Raman scattering counterparts—requires external references for the assignment of the signs of specific chiroptical responses. This need has motivated the development of theoretical models of CPL spectra, beginning with the semiempirical calculations of Schlessinger and Warshel in 1974.<sup>17</sup> The first density-functional theory (DFT) computations were carried out by Coughlin *et al.* in 2008<sup>8</sup> in their examination of iridium (III) complexes. In 2010, Pritchard and Autschbach<sup>18</sup> used DFT to compute Franck-Condon vibrationally resolved absorption, emission, ECD, and CPL bands corresponding to the lowest-energy  $n \rightarrow \pi^*$  transition of the small chiral ketones, *d*-camphorquinone, (*S,S*)-*trans*- $\beta$ -hydrindanone, and (1*R*,5*S*)-*cis*- $\beta$ -hydrindanone, for comparison with well-resolved experimental spectra. They found that the camphorquinone exhibits

<sup>a)</sup>crawdad@vt.edu

little structural variation between the ground and excited states, while the  $n \rightarrow \pi^*$  excitation results in a loss of  $C_2$  symmetry in the *trans*- $\beta$ -hydrindanone as its carbonyl is bent out of the plane of the cyclopentane ring.

Pecul and Ruud<sup>19</sup> also carried out a series of DFT computations of CPL spectra of organic ketones. Their selection of five  $\beta, \gamma$ -enones was directly inspired by the experimental work of Schippers *et al.*,<sup>20</sup> who reported fascinating variations in the signs of rotational strengths for the lowest-energy ECD  $n \rightarrow \pi^*$  and CPL  $\pi^* \rightarrow n$  transitions. Pecul and Ruud found that three of the five compounds—(1*S*,3*R*)-4-methyleneadamantan-2-one, (1*R*)-7-methylenebicyclo[2.2.1]heptan-2-one, and (1*S*)-2-methylenebicyclo[2.2.1]heptan-7-one—manifest two conformers in the excited state corresponding to different orientations of the carbonyl group relative to the bridgehead carbon of the cage, and each conformer yields an opposite-sign rotatory strength. For these three compounds, the overall sign of the CPL transition was found to depend on which structure was lower in energy and disagreement was observed for two of the compounds (the methyleneadamantan-2-one and the methylenebicyclo[2.2.1]heptan-7-one) between the Becke three-parameter exchange function and Lee-Yang-Parr correlation functional (B3LYP) and its counterpart corrected using the Coulomb attenuating method (CAM-B3LYP).<sup>23</sup> Furthermore, while CAM-B3LYP predictions of dipole and rotatory strengths were closer to experiment for four of the five compounds, B3LYP dissymmetry factors—which are proportional to the ratio of the two transition strengths—were closer to the measured values, apparently due to cancellation of errors. For the smallest of their  $\beta, \gamma$ -enones, (1*R*,4*R*)-norbornenone, Pecul and Ruud also optimized the ground and excited states using the second-order coupled cluster method (CC2), implemented for greater computational efficiency using the resolution-of-the-identity approach (RI-CC2). Although they found that RI-CC2 produced a significantly longer C=O bond length in the excited state as compared to DFT, CAM-B3LYP and RI-CC2 CPL rotatory strengths (the latter computed using the B3LYP optimized excited-state geometry) agreed well with each other but were not as close as B3LYP to the experimental data.

The most recent theoretical CPL simulations include those of Longhi *et al.*,<sup>24</sup> for a series of bicyclic ketones, again focusing on the lowest-energy  $n \rightarrow \pi^*$  transition using DFT (CAM-B3LYP). Similarly to Pecul and Ruud, they found that, for compounds with more than one excited-state conformer, the sign of the CPL rotatory strengths depended primarily on which was lower in energy, as distinguished by the direction of puckering of the C=O moiety. For camphor, two such conformers were identified, while for 5-oxocamphor, which has two carbonyls, four minimum-energy structures compete. Finally, we note the use of the B3LYP functional by Shen *et al.* in the analysis of photophysical emission of organometallic helicenes in order to elucidate the influence of platinum centers on the compounds' CPL spectra and other chiroptical properties.<sup>25</sup>

The purpose of the present study is twofold. First, we consider the importance of higher-order electron correlation effects on the sign and structure of simulated CPL spectra by

application of coupled cluster theory—particularly on the geometries and energy ordering of key excited states—for the first time at the coupled cluster singles and doubles (CCSD) level of theory for the ground state and the equation-of-motion CCSD (EOM-CCSD) level for excited states. Second, for selected compounds, we go beyond the lowest-energy transition and consider the requirements of a robust theoretical simulation of CPL bands corresponding to non-valence excited states.

## II. COMPUTATIONAL DETAILS

From the EOM-CC perspective, transition strengths are computed using the eigenfunctions of the similarity-transformed Hamiltonian, *via*,<sup>26–30</sup>

$$e^{-\hat{T}} \hat{H} e^{\hat{T}} \hat{R}_n |0\rangle = \bar{H} \hat{R}_n |0\rangle = E_n \hat{R}_n |0\rangle \quad (1)$$

and

$$\langle 0 | \hat{L}_n \bar{H} = E_n \langle 0 | \hat{L}_n, \quad (2)$$

where  $|0\rangle$  is the single-determinant reference function,  $\hat{T}$  is the ground-state cluster operator, and  $\hat{R}_n$  and  $\hat{L}_n$  represent excitation and de-excitation cluster operators, respectively. Unlike variational methods such as configuration interaction, the left- and right-hand eigenfunctions are not simply adjoints of each other due to the non-Hermitian nature of  $\bar{H}$ , though the excitation energies,  $E_n$ , are identical. This leads to the distinct left- and right-hand transition-moment expressions,

$$\langle \Psi_0 | \vec{A} | \Psi_n \rangle = \langle 0 | (1 + \hat{\Lambda}) e^{-\hat{T}} \vec{A} e^{\hat{T}} \hat{R}_n |0\rangle \quad (3)$$

and

$$\langle \Psi_n | \vec{B} | \Psi_0 \rangle = \langle 0 | \hat{L}_n e^{-\hat{T}} \vec{B} e^{\hat{T}} |0\rangle, \quad (4)$$

where  $|\Psi_0\rangle$  and  $|\Psi_n\rangle$  are the ground- and  $n$ th-excited-state, respectively,  $\vec{A}$  and  $\vec{B}$  are (vector) property operators, and  $\hat{\Lambda}$  denotes the cluster de-excitation operator associated with the left-hand ground-state wave function. Although the corresponding transition strengths (the dot product of the above moment expressions) are not size intensive in the truncated EOM-CC approach,<sup>27,30</sup> such errors are not likely to be significant for the relatively small molecular systems considered in this work. For the dipole transition strengths required for absorption and fluorescence, both  $\vec{A}$  and  $\vec{B}$  are chosen to be the electric dipole operator, and CD and CPL rotatory strengths require the mixed response function between the electric dipole operator and the magnetic dipole operator,  $\vec{m}$ . While the choice of length ( $\vec{r}$ ) or velocity ( $\vec{p}$ ) representation for the electric dipole operator is inconsequential for exact wave functions, the use of finite basis sets leads to differences between the computed transition strengths (as well as arbitrary origin dependence for the rotatory strengths calculated using the length representation) for all quantum chemical methods. However, coupled cluster transition strengths exhibit differences between the two representations even in a complete basis due to the lack of variational optimization of the CC energy with respect to the molecular orbitals used to represent the correlated wave function. (Note that this problem also plagues truncated configuration interaction methods.) Thus, in

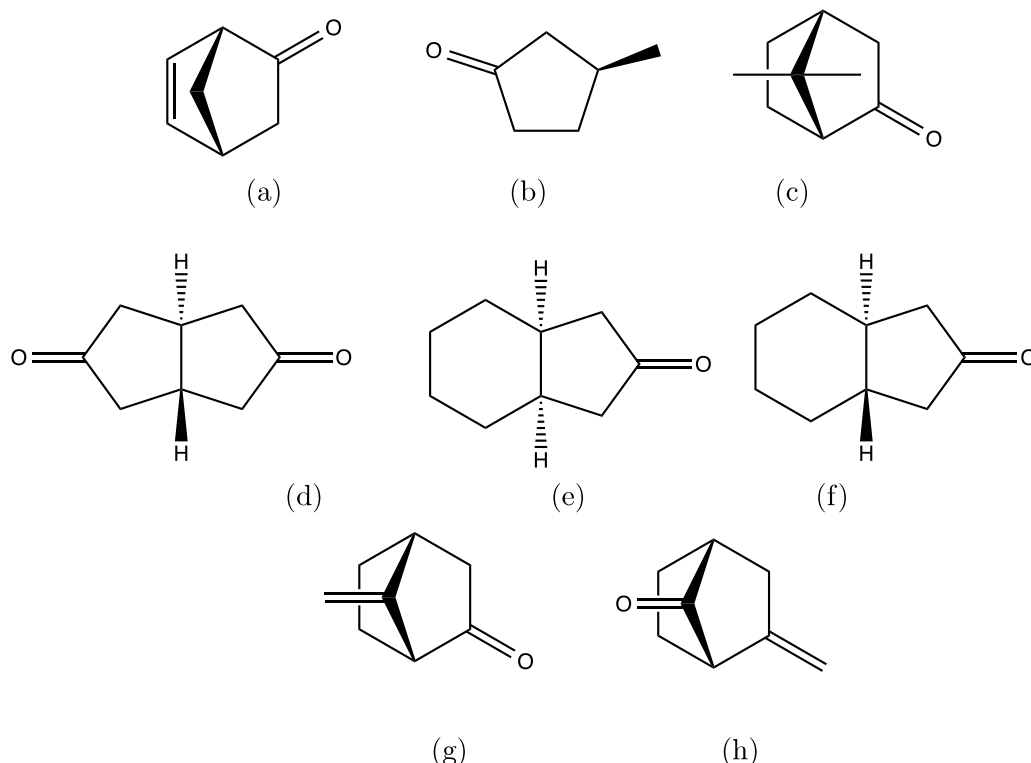


FIG. 1. Structures of (a) (1*R*,4*R*)-norbornenone, (b) (*S*)-3-methylcyclopentanone, (c) (1*R*,4*R*)- $\alpha$ -fenchocampherone, (d) *trans*-bicyclo[3.3.0]octane-3,7-dione, (e) (1*R*,5*S*)-*cis*- $\beta$ -hydrindanone, (f) (*S,S*)-*trans*- $\beta$ -hydrindanone, (g) (1*R*)-7-methylenebicyclo[2.2.1]heptan-2-one, and (h) (1*S*)-2-methylenebicyclo[2.2.1]heptan-7-one.

this work, when computing the dipole and rotational strengths, both the length and velocity formalisms were obtained, with the latter provided in the supplementary material.<sup>31</sup>

We have carried out ECD and CPL calculations for the series of organic ketones shown in Figure 1. All ground-state geometries were optimized using the B3LYP<sup>21,22,32</sup> and CAM-B3LYP<sup>23</sup> functionals in conjunction with the aug-cc-pVDZ<sup>33,34</sup> basis set. The relevant excited states were optimized with the corresponding time-dependent DFT (TDDFT)<sup>35</sup> and employing the same basis set and functional. For two systems—(1*R*,4*R*)-norbornenone and (*S*)-3-methylcyclopentanone—we also performed coupled cluster level optimizations of the geometries, using CCSD for the ground states and EOM-CCSD for the excited states, again with the aug-cc-pVDZ basis set.<sup>26,36–38</sup> Structural optimizations were considered converged when the maximum and root-mean-squared values of the Cartesian gradient vector fell below  $10^{-4}E_h/a_0$ . Analytic gradient methods were used for both DFT- and coupled-cluster-based optimizations.<sup>38</sup> All electrons were correlated in the coupled cluster structural optimizations, while the 1*s* core orbitals on all carbon and oxygen atoms were held frozen in the coupled cluster transition-property computations. DFT computations were performed using Gaussian-09,<sup>39</sup> and all coupled-cluster level results were obtained using the PSI4 quantum chemical program.<sup>40</sup>

Dipole absorption strengths and ECD rotatory strengths were obtained for the lowest several excited states in the TDDFT and EOM-CCSD approximations at the optimized ground state geometry of each structure using the aug-cc-pVDZ

basis set. Similarly, dipole emission and CPL rotatory strengths were computed using the same quantum chemical methods at the corresponding excited-state geometries. In addition to calculating the dipole and rotational strengths, we also computed the dissymmetry factor,<sup>18–20</sup>

$$g_x \equiv \frac{4R_x}{D_x}, \quad (5)$$

where  $R$  is the rotational strength (RS) and  $D$  is the dipole strength (DS), and the subscript  $x = a, e$  indicates either absorption (ECD) or emission (CPL).

### III. RESULTS AND DISCUSSION

#### A. Optimized excited-state structures: (1*R*,4*R*)-norbornenone and (*S*)-3-methylcyclopentanone

The optimization of electronically excited states is often cumbersome and computationally expensive, particularly for advanced many-body methods such as coupled cluster theory. It would therefore be advantageous to identify less expensive, yet acceptably accurate alternatives to complete CC optimizations. With this goal in mind, we have carried out EOM-CCSD/aug-cc-pVDZ optimizations of the ground and first three excited states of (1*R*,4*R*)-norbornenone, as well as the ground and first two excited states of (*S*)-3-methylcyclopentanone, for comparison to corresponding B3LYP/aug-cc-pVDZ optimizations. (Complete coordinates for all structures are given in the supplementary material.<sup>31</sup>)

In the work by Pecul and Ruud,<sup>19</sup> they observed that the RI-CC2 optimized structure of the first ( $n \rightarrow \pi^*$ ) excited state of norbornenone differed from its B3LYP counterpart primarily in the C=O bond distance, with CC2 yielding a much longer value of 1.360 Å vs. 1.267 Å with B3LYP (and 1.264 Å with CAM-B3LYP). Upon comparison with the first excited state of formaldehyde, which also arises from an  $n \rightarrow \pi^*$  transition, they concluded that the CC2 and B3LYP results likely bracketed the “true” bond length, which they estimated to be ca. 1.295 Å. It is thus noteworthy that the EOM-CCSD/aug-cc-pVDZ optimized structure of this state of (1*R*,4*R*)-norbornenone exhibits a C=O bond length of 1.296 Å, in nearly perfect agreement with the estimate by Pecul and Ruud. All other geometrical parameters, including the C=C distance and key dihedral angles, are essentially identical between EOM-CCSD and both B3LYP and CAM-B3LYP.

Similarly good agreement in the structures obtained with DFT and CC methods is found for the second and third excited states of (1*R*,4*R*)-norbornenone. According to EOM-CCSD/aug-cc-pVDZ, these states exhibit a contraction of the C=O bond to 1.181 Å (second excited state) and 1.189 Å (third) as compared to 1.215 Å in the ground state. The C=C distance, however, increases in both states to 1.429 Å (second) and 1.404 Å (third) vs. 1.358 Å in the ground state, indicating that these states involve  $\pi \rightarrow \pi^*$  transition character. At the same time, the carbonyl distorts only slightly from planarity with the C—C—C plane to which it is connected in both states—slightly away from the bridgehead carbon atom in the second excited state and slightly toward the bridgehead in the third. The largest (but still minor) difference in the EOM-CCSD vs. B3LYP and CAM-B3LYP structures arises for the C=C distance, with the DFT methods yielding 1.446 Å and 1.448 Å, respectively, for the second excited state and 1.387 Å and 1.385 Å for the third.

For (*S*)-3-methylcyclopentanone, we again find that the B3LYP and EOM-CCSD optimized structures of all three states—ground and first two excited states—are very similar,

with the largest difference occurring in the C=O bond length in the first ( $n \rightarrow \pi^*$ ) excited state: EOM-CCSD yields a bond length of 1.313 Å, only 0.017 Å longer than that given by B3LYP. In addition, EOM-CCSD yields slightly greater pyramidalization around the carbonyl carbon in the first excited state, with the C=O moiety bent away from the C—C—C plane by 37° vs. 33° with B3LYP. For the second excited state, the structures produced by EOM-CCSD and B3LYP are essentially identical, with both methods in agreement that the C=O bond distance is *shorter* than in the ground state (1.194 Å vs. 1.217 Å at the EOM-CCSD/aug-cc-pVDZ level of theory) and that no pyramidalization of the carbonyl carbon occurs. Analysis of the EOM-CCSD excited-state wave function and TDDFT orbital transition vectors for this state reveal that it exhibits strong Rydberg character involving the 3*s* orbital of the oxygen atom. Thus, the ground and second excited state structures are similar, apart from the contraction of the C=O bond.

Absorption and emission data computed using EOM-CCSD for (1*R*,4*R*)-norbornenone and (*S*)-3-methylcyclopentanone using the above optimized structures are given in Tables I and II, respectively. For the first excited state of (1*R*,4*R*)-norbornenone, the choice of optimized ground- and excited-state geometries makes little difference, with the largest discrepancy occurring for the dipole strength:  $1716 \times 10^{-40}$  cgs using the CC geometries vs.  $1752 \times 10^{-40}$  cgs using the DFT geometries. However, even this shift is minor and ultimately has minimal impact on the resulting absorption dissymmetry factor. The emission data for the first excited state, on the other hand, show a larger dependence on the choice of optimized excited-state geometry with the B3LYP structures yielding significantly larger values than with the EOM-CCSD structures for the excitation energy (2.94 vs. 2.85 eV, respectively), rotatory strength (21.5 vs.  $12.5 \times 10^{-40}$  cgs), and dipole strength (2389 vs.  $1338 \times 10^{-40}$  cgs). The source of this difference lies, of course, in the longer C=O bond distance (and somewhat less on the larger pyramidalization of the carbonyl carbon) predicted by

TABLE I. EOM-CCSD/aug-cc-pVDZ electronic transition data for the ground and first three excited states of (1*R*,4*R*)-norbornenone. Absorption data were computed using the CCSD or B3LYP optimized ground-state optimized geometries, while emission data were obtained at the corresponding EOM-CCSD or B3LYP (TD-DFT) structures. Reported rotational strengths were computed using the length representation of the electric dipole operator.

Geometry	Transition	Energy (eV)	RS ( $10^{-40}$ cgs)	DS ( $10^{-40}$ cgs)	$g_x$ ( $10^{-3}$ cgs)
CCSD	G $\rightarrow$ 1	4.26	34.06	1716	79.40
B3LYP	G $\rightarrow$ 1	4.29	34.63	1752	79.08
CCSD	G $\leftarrow$ 1	2.85	12.52	1338	37.44
B3LYP	G $\leftarrow$ 1	2.94	21.46	2389	35.93
CCSD	G $\rightarrow$ 2	6.00	-8.380	1042	-32.18
B3LYP	G $\rightarrow$ 2	6.00	-10.06	774.6	-51.92
CCSD	G $\leftarrow$ 2	4.58	61.18	20620	11.87
B3LYP	G $\leftarrow$ 2	4.93	37.31	16750	8.910
CCSD	G $\rightarrow$ 3	6.31	28.26	27250	4.149
B3LYP	G $\rightarrow$ 3	6.33	29.78	26210	4.544
CCSD	G $\leftarrow$ 3	5.62	8.128	21600	1.505
B3LYP	G $\leftarrow$ 3	5.76	19.00	25250	3.011



TABLE II. EOM-CCSD/aug-cc-pVDZ electronic transition data for the ground and first two excited states of (*S*)-3-methylcyclopentanone. Absorption data were computed using the CCSD or B3LYP optimized ground-state optimized geometries, while emission data were obtained at the corresponding EOM-CCSD or B3LYP (TD-DFT) structures. Reported rotational strengths were computed using the length representation of the electric dipole operator.

Geometry	Transition	Energy (eV)	RS ( $10^{-40}$ cgs)	DS ( $10^{-40}$ cgs)	$g_x$ ( $10^{-3}$ cgs)
CCSD	G $\rightarrow$ 1	4.25	-8.884	74.29	-478.3
B3LYP	G $\rightarrow$ 1	4.28	-8.448	66.83	-505.7
CCSD	G $\leftarrow$ 1	3.04	-6.882	986.5	-27.91
B3LYP	G $\leftarrow$ 1	3.21	-6.973	849.5	-32.83
CCSD	G $\rightarrow$ 2	6.32	8.826	10 020	3.524
B3LYP	G $\rightarrow$ 2	6.32	8.285	9 930	3.337
CCSD	G $\leftarrow$ 2	6.05	8.380	10 310	3.250
B3LYP	G $\leftarrow$ 2	6.11	7.738	9 204	3.363

EOM-CCSD. However, the errors in the rotatory and dipole strengths introduced by the use of the B3LYP geometry largely cancel in the emission dissymmetry factor, which differs by ca.  $1.5 \times 10^{-3}$  cgs between the two structures. In addition, the dissymmetry factor decreases by a factor of two between absorption and emission, which reflects the structural changes noted above.

For the second excited state of (1*R*,4*R*)-norbornenone, somewhat larger differences appear between the use of CC or B3LYP geometries. For the second state, for example, while the EOM-CCSD excitation energies are identical for the two structures, the rotatory strengths and dipole strengths are more sensitive to small perturbations in the structure, leading to a sizeable quantitative discrepancy in the corresponding dissymmetry factor of  $19.74 \times 10^{-3}$  cgs between the structures. For the corresponding emission, the shifts in the excitation energy (0.35 eV), rotatory strength ( $23.87 \times 10^{-40}$  cgs), and dipole strengths ( $3870 \times 10^{-40}$  cgs) are even larger, though these mostly cancel in the dissymmetry factor, which differs by less than  $3 \times 10^{-3}$  cgs. The third excited state, on the other hand, is better behaved, with the largest differences between the CC and B3LYP geometries appearing in the rotatory strength of the emission ( $8.128 \times 10^{-40}$  vs.  $19.00 \times 10^{-40}$  cgs, respectively). This leads to a factor of two difference between the dissymmetry factor for the transition, but still only a small shift in absolute terms ( $1.506 \times 10^{-3}$  cgs).

Similar observations may be made for the (*S*)-3-methylcyclopentanone absorption and emission data collected in Table II. For example, the excitation energies for both the first and second excited states shift by less than 0.04 eV between the two choices of optimized geometries. The rotatory strengths exhibit similarly minor changes, and it is noteworthy that the two states give opposite-sign ECD signals. The dipole strengths exhibit somewhat larger differences, though the transition to the first excited state remains weak regardless of the choice of structure, as expected for an  $n \rightarrow \pi^*$  transition. The dipole strength for the second excited state is two orders of magnitude larger than for the first state, again as expected due to the similarity with the ground-state structure, but the choice of optimized geometries leads to a shift of less than 1% in the computed values. The impact of the observed shifts on the absorption dissymmetry factors, however, is, again

relatively minor, particularly for the second excited state. Furthermore, the small structural changes between the ground and second state described above are also reflected in the small difference in the absorption and emission dissymmetry factors ( $3.524$  vs.  $3.250 \times 10^{-3}$  cgs, respectively, using the EOM-CCSD geometries), whereas the difference is more than an order of magnitude larger for the first excited state ( $-478.3$  vs.  $-27.91 \times 10^{-3}$  cgs) due to the concomitantly larger geometry distortions.

Although we do not have sufficient data to separate the errors introduced by the use of the approximate DFT vs. EOM-CC optimized excited-state structures as compared to errors associated with the use of DFT vs. EOM-CC transition strengths, we conclude from the above observations that the DFT optimized structures are sufficient for obtaining reasonably accurate EOM-CC dipole strengths, rotatory strengths, and especially dissymmetry factors for most cases. Thus, we have made use of B3LYP/aug-cc-pVDZ ground- and excited-state optimized geometries for subsequent EOM-CCSD and CAM-B3LYP calculations for all of the remaining test cases, though we necessarily keep in mind that some cases may be problematic and errors associated with the excited-state geometries may occur.

## B. (1*R*,4*R*)- $\alpha$ -fenchocampherone

Table III reports electronic transition data for the ground and first three excited states of (1*R*,4*R*)- $\alpha$ -fenchocampherone. The B3LYP/aug-cc-pVDZ geometries (coordinates given in the supplementary material<sup>31</sup>) follow the typical trends for such ketones. Due to its  $n \rightarrow \pi^*$  character, the first excited states exhibit an extension of the C=O bond from 1.212 Å to 1.286 Å, as well as bending of the carbonyl away from the bridgehead carbon. The second and third states, on the other hand, involve significant Rydberg character associated with the oxygen atom, and thus, their structures are closer to that of the ground state, with C=O bond lengths of 1.192 and 1.190 Å, respectively, and planarity around the carbonyl.

As expected, B3LYP typically underestimates transition energies relative to EOM-CCSD, though CAM-B3LYP largely corrects this discrepancy for the three excited states considered here. More interesting, however, is the corresponding pattern

TABLE III. Electronic transition data for the ground and first three excited states of (1*R*,4*R*)- $\alpha$ -fenchocampherone obtained using EOM-CCSD, B3LYP, and CAM-B3LYP with the aug-cc-pVDZ basis set. Reported rotational strengths were obtained using the length representation of the electric dipole operator.

Method	Transition	Energy (eV)	RS ( $10^{-40}$ cgs)	DS ( $10^{-40}$ cgs)	$g_x$ ( $10^{-3}$ cgs)
EOM-CCSD	G $\rightarrow$ 1	4.31	5.810	126.1	184.3
B3LYP	G $\rightarrow$ 1	4.17	8.038	206.7	155.5
CAM-B3LYP	G $\rightarrow$ 1	4.26	5.822	142.1	163.8
EOM-CCSD	G $\leftarrow$ 1	3.04	1.147	1279	3.586
B3LYP	G $\leftarrow$ 1	2.96	2.565	1118	9.180
CAM-B3LYP	G $\leftarrow$ 1	3.03	1.676	1092	6.141
EOM-CCSD	G $\rightarrow$ 2	6.32	6.889	8311	3.316
B3LYP	G $\rightarrow$ 2	5.57	-4.553	3838	-4.746
CAM-B3LYP	G $\rightarrow$ 2	6.36	5.881	6971	3.375
EOM-CCSD	G $\leftarrow$ 2	6.01	6.642	8482	3.132
B3LYP	G $\leftarrow$ 2	5.30	-5.557	4703	-4.726
CAM-B3LYP	G $\leftarrow$ 2	6.06	5.463	7055	3.097
EOM-CCSD	G $\rightarrow$ 3	6.82	-0.1304	688.2	-0.7576
B3LYP	G $\rightarrow$ 3	6.00	1.701	762.3	8.926
CAM-B3LYP	G $\rightarrow$ 3	6.84	0.5237	839.9	2.494
EOM-CCSD	G $\leftarrow$ 3	6.48	0.01313	1202	0.04369
B3LYP	G $\leftarrow$ 3	5.72	2.183	962.6	9.072
CAM-B3LYP	G $\leftarrow$ 3	6.52	0.8763	1124	3.118

in the dipole and rotatory strengths, with CAM-B3LYP values typically shifted back toward their EOM-CCSD counterparts as compared to B3LYP. For the absorption to the second excited state, for example, EOM-CCSD yields a dipole strength of  $8311 \times 10^{-40}$  cgs, while B3LYP predicts a value of less than half that of  $3838 \times 10^{-40}$  cgs. CAM-B3LYP, however, yields a value much closer to EOM-CCSD at  $6971 \times 10^{-40}$  cgs. Similarly for rotatory strengths, CAM-B3LYP tends to fall closer to EOM-CCSD than B3LYP, *e.g.*, for the absorption to the first excited state where CAM-B3LYP and EOM-CCSD give values near  $5.8 \times 10^{-40}$  cgs, while B3LYP yields a value roughly 40% larger at  $8.0 \times 10^{-40}$  cgs. Furthermore, for the absorption and emission between the ground and second excited state, B3LYP yields a qualitatively incorrect rotatory strength—and thus, an incorrect dissymmetry factor—with a prediction of a negative value vs. the positive values given by both EOM-CCSD and CAM-B3LYP.

An additional point of disagreement appears between coupled cluster and density functional methods for (1*R*,4*R*)- $\alpha$ -fenchocampherone. In particular, for the absorption from the ground state to the third excited state, the rotatory strength is negative according to EOM-CCSD and positive according to both B3LYP and CAM-B3LYP—though all three methods predict the transition strength to be small—leading, of course, to opposite sign dissymmetry factors between CC and DFT. Finally, we note that, while the choice of length vs. velocity representations of the electric dipole operator makes little difference for most of the EOM-CCSD predictions, the emission from the first excited state exhibits a qualitative discrepancy between the two. The length representation (Table III) gives a value of  $+1.147 \times 10^{-40}$  cgs (in agreement with both B3LYP and CAM-B3LYP), while the velocity representation gives  $-3.493 \times 10^{-40}$  cgs. (Velocity

representation data are provided for all compounds in the supplementary material.<sup>31</sup>)

### C. $\beta$ -hydrindanone

Table IV reports CC and DFT electronic transition data for (1*R*,5*S*)-*cis*- $\beta$ -hydrindanone, which exhibits similar patterns to those of (1*R*,4*R*)- $\alpha$ -fenchocampherone in that CAM-B3LYP typically yields excitation energies, dipole strengths, and rotatory strengths closer to EOM-CCSD than does B3LYP. Like (1*R*,4*R*)- $\alpha$ -fenchocampherone, the first excited state is largely of  $n \rightarrow \pi^*$  character, while the second and third states are more diffuse. This is borne out by their structures: the first excited state exhibits a C=O bond length of 1.297 Å, more than 0.08 Å longer than that of the ground state, while the second and third excited states have C=O bonds of 1.198 and 1.197 Å, respectively. The most significant discrepancy among the three methods occurs for the second excited state, for which B3LYP yields negative rotatory strengths in both absorption and emission, whereas EOM-CCSD and CAM-B3LYP give positive rotatory strengths for this state. Examination of the velocity gauge data for emission from the second excited state reveals a change in sign for the CAM-B3LYP rotatory strength, bringing it in agreement with the B3LYP results. However, the CAM-B3LYP and EOM-CCSD rotatory strengths are very small—less than  $1 \times 10^{-40}$  cgs in magnitude—for both gauge representations, and the CAM-B3LYP data are much closer to EOM-CCSD than B3LYP despite differences in sign.

Similarly, Table V reports transition data for the first excited state of (*S,S*)-*trans*- $\beta$ -hydrindanone. (Unlike (1*R*,4*R*)- $\alpha$ -fenchocampherone and (1*R*,5*S*)-*cis*- $\beta$ -hydrindanone, we were unable to optimize higher lying states for this molecule.) Like its *cis* counterpart, the first excited state is characterized

TABLE IV. Electronic transition data for the ground and first three excited states of (1*R*,5*S*)-*cis*- $\beta$ -hydrindanone obtained using EOM-CCSD, B3LYP, and CAM-B3LYP with the aug-cc-pVDZ basis set. Reported rotational strengths were obtained using the length representation of the electric dipole operator.

Method	Transition	Energy (eV)	RS ( $10^{-40}$ cgs)	DS ( $10^{-40}$ cgs)	$g_x$ ( $10^{-3}$ cgs)
EOM-CCSD	G $\rightarrow$ 1	4.26	8.220	76.17	431.7
B3LYP	G $\rightarrow$ 1	4.14	11.59	135.7	341.6
CAM-B3LYP	G $\rightarrow$ 1	4.22	8.725	83.99	415.5
EOM-CCSD	G $\leftarrow$ 1	3.23	7.245	803.4	36.07
B3LYP	G $\leftarrow$ 1	3.17	9.734	743.0	52.41
CAM-B3LYP	G $\leftarrow$ 1	3.25	8.084	691.3	46.78
EOM-CCSD	G $\rightarrow$ 2	6.32	0.6181	9016	0.2743
B3LYP	G $\rightarrow$ 2	5.61	-4.092	5104	-3.207
CAM-B3LYP	G $\rightarrow$ 2	6.34	0.3677	8063	0.1824
EOM-CCSD	G $\leftarrow$ 2	6.09	0.8460	8082	0.4187
B3LYP	G $\leftarrow$ 2	5.41	-5.350	5026	-4.257
CAM-B3LYP	G $\leftarrow$ 2	6.11	0.1108	7145	0.06203
EOM-CCSD	G $\rightarrow$ 3	6.77	7.342	3311	8.870
B3LYP	G $\rightarrow$ 3	5.98	6.096	3114	7.831
CAM-B3LYP	G $\rightarrow$ 3	6.77	6.808	3579	7.608
EOM-CCSD	G $\leftarrow$ 3	6.48	6.099	3366	7.248
B3LYP	G $\leftarrow$ 3	5.72	8.896	4477	7.948
CAM-B3LYP	G $\leftarrow$ 3	6.49	6.440	3876	6.646

by an  $n \rightarrow \pi^*$  transition, resulting in extension of the C=O bond from 1.212 Å to 1.295 Å. Furthermore, the rotatory strengths, dipole strengths, and dissymmetry factors for the first excited state of both *cis* and *trans* isomers of  $\beta$ -hydrindanone compare closely, *e.g.*, at the EOM-CCSD/aug-cc-pVDZ level of theory, the absorption and emission symmetry factors of *cis* (*trans*) isomers are ( $\times 10^{-40}$  cgs) 431.7 (390.7) and 36.07 (34.87), respectively, which suggest that their absorption (CD) and emission (CPL) signatures will be similar. This observation agrees with Pritchard and Autschbach's analysis<sup>18</sup> of the vibronic structure of the first excited state of (1*R*,5*S*)-*cis*- $\beta$ -hydrindanone, *viz.*, that the CPL emission signature is primarily due to the chirality around the carbonyl moiety.

#### D. *Trans*-bicyclo[3.3.0]octane-3,7-dione

The ground state of *trans*-bicyclo[3.3.0]octane-3,7-dione has  $C_{2h}$  point-group symmetry and is thus achiral. However,  $n \rightarrow \pi^*$  excitation results in elongation of one of its C=O bonds from 1.209 Å to 1.292 Å, as well as puckering of the

carbonyl away from planarity. This puckering can proceed in either direction off the  $C_2$  symmetry axis and toward the horizontal plane of the ground state, yielding a non-symmetric, and thus chiral, structure. The two resulting enantiomers may be labelled as either *M* or *P* in relation to the central, twisted C—C bond joining the two cyclopentanone rings. The dipole strength of the absorption is relatively large, as shown in Table VI, though the corresponding rotatory strength and dissymmetry factor are both zero in the Franck-Condon (vertical transition) approximation. Emission from the chiral excited state, however, involves significant dipole and rotatory strengths, and the latter is predicted to be negative for the *P* enantiomer and positive for the *M* enantiomer. As observed for the other systems discussed above, CAM-B3LYP gives a value between EOM-CCSD and B3LYP for the rotatory strengths, though EOM-CCSD and B3LYP agree somewhat better for the dipole strengths in this case.

The second excited-state of *trans*-bicyclo[3.3.0]octane-3,7-dione, however, is primarily of oxygen 3*s*-type Rydberg character and thus, retains the same  $C_{2h}$  symmetry of the ground state. In addition, the excited-state character

TABLE V. Electronic transition data for the ground and first excited state of (*S,S*)-*trans*- $\beta$ -hydrindanone obtained using EOM-CCSD, B3LYP, and CAM-B3LYP with the aug-cc-pVDZ basis set. Reported rotational strengths were obtained using the length representation of the electric dipole operator.

Method	Transition	Energy (eV)	RS ( $10^{-40}$ cgs)	DS ( $10^{-40}$ cgs)	$g_x$ ( $10^{-3}$ cgs)
EOM-CCSD	G $\rightarrow$ 1	4.27	11.32	115.9	390.7
B3LYP	G $\rightarrow$ 1	4.14	15.64	213.2	293.5
CAM-B3LYP	G $\rightarrow$ 1	4.23	12.10	122.7	394.2
EOM-CCSD	G $\leftarrow$ 1	3.20	7.738	887.6	34.87
B3LYP	G $\leftarrow$ 1	3.13	11.24	833.4	53.93
CAM-B3LYP	G $\leftarrow$ 1	3.21	8.849	749.4	47.23



TABLE VI. Electronic transition data for the ground and first two excited states of *trans*-bicyclo[3.3.0]octane-3,7-dione obtained using EOM-CCSD, B3LYP, and CAM-B3LYP with the aug-cc-pVDZ basis set. Reported rotational strengths were obtained using the length representation of the electric dipole operator.

Method	Transition	Energy (eV)	RS ( $10^{-40}$ cgs)	DS ( $10^{-40}$ cgs)	$g_x$ ( $10^{-3}$ cgs)
EOM-CCSD	G $\rightarrow$ 1 ( <i>P/M</i> )	4.26	...	400.2	...
B3LYP	G $\rightarrow$ 1 ( <i>P/M</i> )	4.07	...	1040.0	...
CAM-B3LYP	G $\rightarrow$ 1 ( <i>P/M</i> )	4.20	...	426.4	...
EOM-CCSD	G $\leftarrow$ 1 ( <i>P</i> )	3.23	-9.645	943.0	-40.91
B3LYP	G $\leftarrow$ 1 ( <i>P</i> )	3.14	-17.01	1001	-67.94
CAM-B3LYP	G $\leftarrow$ 1 ( <i>P</i> )	3.24	-11.04	807.6	-54.68
EOM-CCSD	G $\leftarrow$ 1 ( <i>M</i> )	3.23	9.645	943.0	40.91
B3LYP	G $\leftarrow$ 1 ( <i>M</i> )	3.14	17.01	1001	67.94
CAM-B3LYP	G $\leftarrow$ 1 ( <i>M</i> )	3.24	11.04	807.6	54.68
EOM-CCSD	G $\rightarrow$ 2	4.31	...	...	...
B3LYP	G $\rightarrow$ 2	4.19	...	...	...
CAM-B3LYP	G $\rightarrow$ 2	4.26	...	...	...
EOM-CCSD	G $\leftarrow$ 2	4.02	...	...	...
B3LYP	G $\leftarrow$ 2	3.92	...	...	...
CAM-B3LYP	G $\leftarrow$ 2	4.00	...	...	...

corresponds to a  $^1B_g$  state, which is a dipole-forbidden transition from the  $^1A_g$  ground state (as well as an allowed, but essentially zero magnetic dipole-transition), as can be seen in Table VI. (We further note that all three states considered here have been confirmed as minima on their respective potential energy surfaces.)

### E. $\beta$ , $\gamma$ -enones

In addition to (1*R*,4*R*)-norbornenone discussed earlier, we considered two additional  $\beta$ , $\gamma$ -enones, (1*R*)-7-methylenebicyclo[2.2.1]heptan-2-one and (1*S*)-2-methylenebicyclo[2.2.1]heptan-7-one, both of which were also analyzed by Pecul and Ruud<sup>19</sup> for comparison with earlier experimental data.<sup>20</sup> They reported that these two molecules exhibit two minima on the

lowest  $n \rightarrow \pi^*$  potential energy surface, distinguished by the direction of pyramidalization of the C=O moiety either away from the C=C bond (to which they referred as **E1**) or toward the C=C bond (**E2**). We have identified these same structures for both (1*R*)-7-methylenebicyclo[2.2.1]heptan-2-one and (1*S*)-2-methylenebicyclo[2.2.1]heptan-7-one, as well as a second valence excited state of each molecule with mixed  $n \rightarrow \pi^*$  and  $\pi \rightarrow \pi^*$  character. In both molecules, this latter state exhibits the same pyramidalization around the C=O as its **E1** counterpart, but much more pronounced elongation of the C=C bond, *e.g.*, in (1*S*)-2-methylenebicyclo[2.2.1]heptan-7-one, the C=C bond is 1.335 Å in the ground state, 1.350 Å in **E1**, and 1.384 Å in the second excited state. The EOM-CC and DFT vertical electronic transition properties for these states are given in Tables VII and VIII.

TABLE VII. Electronic transition data for the ground and first two excited states of (1*R*)-7-methylenebicyclo[2.2.1]heptan-2-one obtained using EOM-CCSD, B3LYP, and CAM-B3LYP with the aug-cc-pVDZ basis set. Reported rotational strengths were obtained using the length representation of the electric dipole operator.

Method	Transition	Energy (eV)	RS ( $10^{-40}$ cgs)	DS ( $10^{-40}$ cgs)	$g_x$ ( $10^{-3}$ cgs)
EOM-CCSD	G $\rightarrow$ 1	4.31	18.74	1149	65.25
B3LYP	G $\rightarrow$ 1	4.12	30.19	2907	41.54
CAM-B3LYP	G $\rightarrow$ 1	4.24	21.84	1525	57.31
EOM-CCSD	G $\leftarrow$ 1 ( <b>E1</b> )	2.99	9.357	1311	28.55
B3LYP	G $\leftarrow$ 1 ( <b>E1</b> )	2.87	18.08	1202	60.19
CAM-B3LYP	G $\leftarrow$ 1 ( <b>E1</b> )	2.96	12.67	1124	45.07
EOM-CCSD	G $\leftarrow$ 1 ( <b>E2</b> )	3.01	-0.8767	2884	-1.216
B3LYP	G $\leftarrow$ 1 ( <b>E2</b> )	2.88	-0.2693	4114	-0.2619
CAM-B3LYP	G $\leftarrow$ 1 ( <b>E2</b> )	2.97	-1.447	3055	-1.895
EOM-CCSD	G $\rightarrow$ 2	6.25	-41.23	4988	-33.06
B3LYP	G $\rightarrow$ 2	5.59	-22.05	3825	-23.07
CAM-B3LYP	G $\rightarrow$ 2	6.25	-48.78	7087	-27.53
EOM-CCSD	G $\leftarrow$ 2	5.14	6.892	899.9	30.64
B3LYP	G $\leftarrow$ 2	3.48	2.061	387.6	21.27
CAM-B3LYP	G $\leftarrow$ 2	4.41	5.529	811.9	27.24

TABLE VIII. Electronic transition data for the ground and first two excited states of (1*S*)-2-methylenebicyclo[2.2.1]heptan-7-one obtained using EOM-CCSD, B3LYP, and CAM-B3LYP with the aug-cc-pVDZ basis set. Reported rotational strengths were obtained using the length representation of the electric dipole operator.

Method	Transition	Energy (eV)	RS ( $10^{-40}$ cgs)	DS ( $10^{-40}$ cgs)	$g_x$ ( $10^{-3}$ cgs)
EOM-CCSD	G $\rightarrow$ 1	4.34	-15.26	947.1	-64.46
B3LYP	G $\rightarrow$ 1	4.10	-25.97	3 004	-34.58
CAM-B3LYP	G $\rightarrow$ 1	4.23	-18.56	1 408	-52.72
EOM-CCSD	G $\leftarrow$ 1 (E1)	2.42	-6.819	1 788	-15.25
B3LYP	G $\leftarrow$ 1 (E1)	2.15	-13.38	1 202	-44.55
CAM-B3LYP	G $\leftarrow$ 1 (E1)	2.30	-9.388	1 395	-26.91
EOM-CCSD	G $\leftarrow$ 1 (E2)	2.60	3.413	2 995	4.558
B3LYP	G $\leftarrow$ 1 (E2)	2.43	2.521	3 923	2.571
CAM-B3LYP	G $\leftarrow$ 1 (E2)	2.52	3.334	3 050.0	4.372
EOM-CCSD	G $\rightarrow$ 2	6.10	30.78	8 588	14.34
B3LYP	G $\rightarrow$ 2	5.45	25.00	7 262	13.77
CAM-B3LYP	G $\rightarrow$ 2	6.07	57.13	36 510	6.258
EOM-CCSD	G $\leftarrow$ 2	4.55	1.023	579.4	7.063
B3LYP	G $\leftarrow$ 2	2.89	-11.90	975.5	-48.78
CAM-B3LYP	G $\leftarrow$ 2	3.82	-0.9672	781.7	-4.949

In agreement with Pecul and Ruud,<sup>19</sup> we find that the vertical absorption from the ground state of (1*R*)-7-methylenebicyclo[2.2.1]heptan-2-one exhibits a positive rotatory strength, while that from the ground state of (1*S*)-2-methylenebicyclo[2.2.1]heptan-7-one is negative. EOM-CCSD yields significantly smaller absolute values of both rotatory and dipole strengths for the absorption than either B3LYP or CAM-B3LYP, but somewhat larger absorption dissymmetry factors. Interestingly, and perhaps only coincidentally, the EOM-CC absorption dissymmetry factors for (1*R*)-7-methylenebicyclo[2.2.1]heptan-2-one and (1*S*)-2-methylenebicyclo[2.2.1]heptan-7-one are almost identical in magnitude (but opposite in sign).

On emission, the **E1** and **E2** structures of (1*R*)-7-methylenebicyclo[2.2.1]heptan-2-one exhibit positive and (small) negative rotatory strengths, respectively, while the dipole strength of **E2** is more than a factor of two larger than that of **E1** with EOM-CCSD. This leads to a nearly two order of magnitude difference in the CPL dissymmetry factors between the two structures. For (1*S*)-2-methylenebicyclo[2.2.1]heptan-7-one, the signs of the rotatory strengths are reversed: the **E1** structure gives a negative transition, while **E2** gives a positive transition. The dipole strengths are significantly larger for **E2** than **E1** for (1*S*)-2-methylenebicyclo[2.2.1]heptan-7-one, though the difference is not so great as for (1*R*)-7-methylenebicyclo[2.2.1]heptan-2-one.

Schippers *et al.*<sup>20</sup> measured both polarized and unpolarized absorption and fluorescence spectra of these compounds in *n*-heptane (and in 1:3 methylcyclohexane/isopentane for the emission spectra of (1*S*)-2-methylenebicyclo[2.2.1]heptan-7-one) at ambient temperature. For the  $n \rightarrow \pi^*$  absorption transition of (1*R*)-7-methylenebicyclo[2.2.1]heptan-2-one, they reported a dipole strength of  $1790 \times 10^{-40}$  cgs and a rotatory strength of  $20.5 \times 10^{-40}$  cgs, leading to a dissymmetry factor of  $45.8 \times 10^{-3}$  cgs. Comparison of these data with those of

Table VII reveals very good agreement with CAM-B3LYP for both the dipole and rotatory strengths ( $1525 \times 10^{-40}$  cgs and  $21.84 \times 10^{-40}$  cgs, respectively), but rather poor agreement with B3LYP for these same values ( $2907 \times 10^{-40}$  cgs and  $30.19 \times 10^{-40}$  cgs, respectively). However, the errors in the latter mostly cancel in the dissymmetry factor, resulting in much better agreement with experiment by B3LYP ( $41.54 \times 10^{-3}$  cgs) than by CAM-B3LYP ( $57.31 \times 10^{-3}$  cgs). EOM-CCSD, on the other hand, gives reasonable agreement with experiment for the rotatory strength ( $18.74 \times 10^{-40}$  cgs) but underestimates the dipole strength resulting in much too large of a dissymmetry factor ( $65.25 \times 10^{-3}$  cgs).

For (1*S*)-2-methylenebicyclo[2.2.1]heptan-7-one, the comparison with experiment is similar. For the  $n \rightarrow \pi^*$  absorption, Schippers *et al.*<sup>20</sup> report a dipole strength of  $1870 \times 10^{-40}$  cgs, a rotatory strength of  $-15.2 \times 10^{-40}$  cgs, and a corresponding dissymmetry factor of  $-32.5 \times 10^{-3}$  cgs. Again, CAM-B3LYP yields better agreement with experiment than B3LYP for the two transition strengths, but the errors in B3LYP mostly cancel to give rather close agreement with experiment for the dissymmetry factor:  $-34.58 \times 10^{-3}$  cgs for B3LYP vs.  $-52.72 \times 10^{-3}$  cgs for CAM-B3LYP. Furthermore, whereas EOM-CCSD gives (providentially) perfect agreement with experiment for the rotatory strength ( $-15.26 \times 10^{-40}$  cgs), it underestimates the dipole strength by a factor of two, giving a  $g_a$  value that is correspondingly too large.

For the fluorescence spectra of (1*R*)-7-methylenebicyclo[2.2.1]heptan-2-one, Schippers *et al.*<sup>20</sup> reported a dissymmetry value of  $15.7 \times 10^{-3}$  cgs, but they described their corresponding value for (1*S*)-2-methylenebicyclo[2.2.1]heptan-7-one of  $< 3 \times 10^{-3}$  cgs as “an upper limit of the degree of circular polarization.” From the (1*R*)-7-methylenebicyclo[2.2.1]heptan-2-one transition data in Table VII, emission from the **E1** structure gives a positive rotatory strength, and thus a positive dissymmetry factor, with EOM-CCSD giving the best agreement with experiment at  $28.55 \times 10^{-3}$  cgs. For

TABLE IX. Adiabatic excitation energies (in eV) at the B3LYP/aug-cc-pVDZ optimized geometries for (1*R*)-7-methylenebicyclo[2.2.1]heptan-2-one and (1*S*)-2-methylenebicyclo[2.2.1]heptan-7-one.

Transition	EOM-CCSD	B3LYP	CAM-B3LYP
(1 <i>R</i> )-7-methylenebicyclo[2.2.1]heptan-2-one			
1 (E1)	3.83	3.76	3.90
1 (E2)	3.88	3.79	3.94
2	6.51	4.91	5.92
(1 <i>S</i> )-2-methylenebicyclo[2.2.1]heptan-7-one			
1 (E1)	3.74	3.50	3.73
1 (E2)	3.68	3.56	3.71
2	6.01	4.44	5.43

(1*S*)-2-methylenebicyclo[2.2.1]heptan-7-one, emission from **E2** gives a positive rotatory strength and dissymmetry factor, with all three theoretical methods giving good agreement with the small experimental limit of  $g_e$ .

However, as pointed out by Pecul and Ruud,<sup>19</sup> the dominance of **E1** vs. **E2** in the fluorescence and CPL spectra depends upon which structure is lower in energy upon *adiabatic* emission. The corresponding energy differences between the ground state and each of **E1** and **E2** (as well as the second excited state) of (1*R*)-7-methylenebicyclo[2.2.1]heptan-2-one and (1*S*)-2-methylenebicyclo[2.2.1]heptan-7-one are given in Table IX. All three methods agree that conformer **E1** of (1*R*)-7-methylenebicyclo[2.2.1]heptan-2-one lies slightly lower in energy than **E2**, with EOM-CCSD predicting the largest difference of only 0.05 eV. For (1*S*)-2-methylenebicyclo[2.2.1]heptan-7-one, however, both EOM-CCSD and CAM-B3LYP predict **E2** to be lower in energy than **E1** (by 0.06 eV, according to EOM-CCSD), whereas B3LYP predicts **E1** to be lower (also by 0.06 eV). Thus, B3LYP would predict a *negative* dissymmetry factor for the polarized emission in (1*S*)-2-methylenebicyclo[2.2.1]heptan-7-one, in disagreement with both the experimentally determined limit and the EOM-CCSD and CAM-B3LYP predictions.

#### IV. CONCLUSIONS

We have carried out the first EOM-CCSD calculations of CPL rotatory strengths for comparison to results from both DFT (B3LYP and CAM-B3LYP) and experiment using a series of eight chiral ketones as a test set. For each case, we obtained optimized structures for up to three excited states, including both valence and Rydberg-type states—the latter being CPL transitions which have not been examined theoretically before. For two of the test molecules—(1*R*,4*R*)-norbornenone and (*S*)-3-methylcyclopentanone—we compared the efficacy of optimizing the excited-state geometries using B3LYP (TD-DFT) vs. EOM-CCSD in order to streamline the determination of the corresponding transition strengths. We observed only minimal differences between the structures obtained using each method, as well as acceptably small differences in vertical transition properties calculated

with EOM-CCSD using the two sets of geometries. Thus, we pursued only B3LYP ground- and excited-state geometry optimizations for the remaining six molecules.

For most of the cases considered here, EOM-CCSD and CAM-B3LYP exhibited relatively good agreement, while B3LYP typically underestimated excitation energies and overestimated rotatory strengths. For one case, (1*R*,4*R*)- $\alpha$ -fenchocampherone, EOM-CCSD and the DFT methods disagreed on the sign of the rotatory strength for the absorption to the third excited state; all other cases exhibited (at least) qualitative agreement between CC and CAM-B3LYP. The choice of length vs. velocity representation of the electric dipole operator made little qualitative or quantitative difference for almost all cases, the only exceptions being the CPL emission from the first excited state of (1*R*,4*R*)- $\alpha$ -fenchocampherone and from the second excited state of (1*R*,5*S*)-*cis*- $\beta$ -hydrindanone.

One test case, *trans*-bicyclo[3.3.0]octane-3,7-dione, exhibits the intriguing phenomenon of having a  $C_{2h}$ -symmetric (and thus achiral) ground state and second excited state, but a  $C_1$  non-symmetric (chiral) first excited state. Thus, the vertical transition from the ground state to the first excited state has a zero rotatory strength, but we predict the corresponding emission to exhibit a strong CPL signal. While the inclusion of vibronic effects in the simulation would lead to non-zero rotatory strengths for the absorption, they would likely remain weak. To our knowledge, this has not yet been investigated experimentally.

Finally, we compared theoretical and experimental ECD and CPL spectral data for two  $\beta,\gamma$ -enones, (1*R*)-7-methylenebicyclo[2.2.1]heptan-2-one and (1*S*)-2-methylenebicyclo[2.2.1]heptan-7-one, which exhibit two conformers on the first excited-state potential energy surface. While CAM-B3LYP provides closer agreement with experiment for both dipole and rotatory absorption strengths than B3LYP, the latter yields better agreement for the corresponding dissymmetry factor due to cancellation of errors. In addition, for these two compounds, EOM-CCSD significantly underestimates the dipole strength of the absorption, resulting in a concomitant overestimation of the related dissymmetry factor. On the other hand, EOM-CCSD yields near-perfect (and fortuitous) agreement with the experimental rotatory strength for (1*S*)-2-methylenebicyclo[2.2.1]heptan-7-one. Finally, both CAM-B3LYP and EOM-CCSD predict the same energy ordering of the two conformers of the first excited state of (1*S*)-2-methylenebicyclo[2.2.1]heptan-7-one, yielding good agreement with experiment for the sign of the CPL transition strength, while B3LYP disagrees qualitatively.

#### ACKNOWLEDGMENTS

This research was supported by Grant Nos. CHE-1058420 and ACI-1147794 from the U.S. National Science Foundation.

<sup>1</sup>L. D. Barron, *Molecular Light Scattering and Optical Activity*, 2nd ed. (Cambridge University Press, Cambridge, UK, 2004).

<sup>2</sup>N. Berova, P. L. Polavarapu, K. Nakanishi, and R. W. Woody, *Comprehensive Chiroptical Spectroscopy* (Wiley, 2012).

<sup>3</sup>M. Pecul and K. Ruud, *Adv. Quantum Chem.* **50**, 185–212 (2005).

<sup>4</sup>J. Autschbach, *Chirality* **21**, E116–E152 (2009).

- <sup>5</sup>T. D. Crawford, in *Comprehensive Chiroptical Spectroscopy*, edited by N. Berova, K. Nakanishi, R. W. Woody, and P. Polavarapu (Wiley, 2012), Vol. 1, pp. 675–697.
- <sup>6</sup>F. S. Richardson and J. P. Riehl, *Chem. Rev.* **77**, 773–792 (1977).
- <sup>7</sup>E. Gussakovskiy, in *Circularly Polarized Luminescence (CPL) of Proteins and Protein Complexes*, edited by C. D. Geddes (Springer, New York, 2008), Vol. 2008, pp. 425–459.
- <sup>8</sup>F. J. Coughlin, M. S. Westrol, K. D. Oylar, N. Byrne, C. Krami, E. Zysman-Colman, M. S. Lowry, and S. Bernhard, *Inorg. Chem.* **47**, 2039–2048 (2008).
- <sup>9</sup>F. C. Spano, Z. Zhao, and S. C. J. Meskers, *J. Chem. Phys.* **120**, 10594–10604 (2004).
- <sup>10</sup>H. G. Brittain and F. S. Richardson, *J. Chem. Phys.* **80**, 2590–2592 (1976).
- <sup>11</sup>A. Salam, *Chem. Phys.* **173**, 123–132 (1993).
- <sup>12</sup>H. P. J. M. Dekkers, C. A. Emeis, and L. J. Oosterhoff, *J. Am. Chem. Soc.* **91**, 4589–4590 (1969).
- <sup>13</sup>H. P. J. M. Dekkers and P. F. Moral, *Tetrahedron: Asymmetry* **4**, 473–478 (1993).
- <sup>14</sup>H. G. Brittain and N. Grinberg, in *Techniques of Chiroptical Spectroscopy*, 3rd ed., edited by J. Cazes (CRC Press, 2005), Chap. 10, pp. 271–294.
- <sup>15</sup>H. Wynberg, E. W. Meijer, J. C. Hummelen, H. P. J. M. Dekkers, P. H. Schippers, and A. D. Carlson, *Nature* **286**, 641–642 (1980).
- <sup>16</sup>E. Castiglioni, S. Abbate, and G. Longhi, *Appl. Spectrosc.* **64**, 1416–1419 (2010).
- <sup>17</sup>J. Schlessinger and A. Warshel, *Chem. Phys. Lett.* **28**, 380–383 (1974).
- <sup>18</sup>B. Pritchard and J. Autschbach, *ChemPhysChem* **11**, 2409–2415 (2010).
- <sup>19</sup>M. Pecul and K. Ruud, *Phys. Chem. Chem. Phys.* **13**, 643–650 (2011).
- <sup>20</sup>P. H. Schippers, J. P. M. van der Ploeg, and H. P. J. M. Dekkers, *J. Am. Chem. Soc.* **105**, 84–89 (1983).
- <sup>21</sup>C. Lee, W. Yang, and R. G. Parr, *Phys. Rev. B* **37**, 785–789 (1988).
- <sup>22</sup>P. J. Stephens, F. J. Devlin, C. F. Chabalowski, and M. J. Frisch, *J. Phys. Chem.* **98**, 11623–11627 (1994).
- <sup>23</sup>T. Yanai, D. P. Tew, and N. C. Handy, *Chem. Phys. Lett.* **393**, 51–57 (2004).
- <sup>24</sup>G. Longhi, E. Castiglioni, S. Abbate, F. Lebon, and D. A. Lightner, *Chirality* **25**, 589–599 (2013).
- <sup>25</sup>C. Shen, E. Anger, M. Srebro, N. Vanthuyne, K. K. Deol, T. D. Jefferson, G. Muller, J. A. G. Williams, L. Toupet, C. Roussel, J. Autschbach, R. Réau, and J. Crassous, *Chem. Sci.* **5**, 1915–1927 (2014).
- <sup>26</sup>J. F. Stanton and R. J. Bartlett, *J. Chem. Phys.* **98**, 7029–7039 (1993).
- <sup>27</sup>H. Koch, R. Kobayashi, A. S. de Merás, and P. Jørgensen, *J. Chem. Phys.* **100**, 4393–4400 (1994).
- <sup>28</sup>H. Koch and P. Jørgensen, *J. Chem. Phys.* **93**, 3333–3344 (1990).
- <sup>29</sup>H. Koch, H. J. Aa. Jensen, P. Jørgensen, and T. Helgaker, *J. Chem. Phys.* **93**, 3345–3350 (1990).
- <sup>30</sup>F. Pawłowski, J. Olsen, and P. Jørgensen, *J. Chem. Phys.* **142**, 114109 (2015).
- <sup>31</sup>See supplementary material at <http://dx.doi.org/10.1063/1.4917521> for Cartesian coordinates (in Ångströms), adiabatic excitation energies, and velocity-gauge transition strengths and dissymmetry factors for all states of all test structures examined in this work.
- <sup>32</sup>A. D. Becke, *J. Chem. Phys.* **98**, 5648–5652 (1993).
- <sup>33</sup>T. H. Dunning, *J. Chem. Phys.* **90**, 1007 (1989).
- <sup>34</sup>T. H. Dunning, K. A. Peterson, and A. K. Wilson, *J. Chem. Phys.* **114**, 9244–9253 (2001).
- <sup>35</sup>M. E. Casida, in *Recent Advances in Density Functional Methods*, edited by D. P. Chong (World Scientific, Singapore, 1995), Vol. 1.
- <sup>36</sup>T. D. Crawford and H. F. Schaefer, in *Reviews in Computational Chemistry*, edited by K. B. Lipkowitz and D. B. Boyd (VCH Publishers, New York, 2000), Vol. 14, Chap. 2, pp. 33–136.
- <sup>37</sup>R. J. Bartlett, in *Geometrical Derivatives of Energy Surfaces and Molecular Properties*, edited by P. Jørgensen and J. Simons (D. Reidel, Dordrecht, 1986), pp. 35–61.
- <sup>38</sup>J. F. Stanton and J. Gauss, *J. Chem. Phys.* **99**, 8840–8847 (1993).
- <sup>39</sup>M. J. Frisch, G. W. Trucks, H. B. Schlegel, G. E. Scuseria, M. A. Robb, J. R. Cheeseman, G. Scalmani, V. Barone, B. Mennucci, G. A. Petersson, H. Nakatsuji, M. Caricato, X. Li, H. P. Hratchian, A. F. Izmaylov, J. Bloino, G. Zheng, J. L. Sonnenberg, M. Hada, M. Ehara, K. Toyota, R. Fukuda, J. Hasegawa, M. Ishida, T. Nakajima, Y. Honda, O. Kitao, H. Nakai, T. Vreven, J. A. Montgomery, Jr., J. E. Peralta, F. Ogliaro, M. Bearpark, J. J. Heyd, E. Brothers, K. N. Kudin, V. N. Staroverov, R. Kobayashi, J. Normand, K. Raghavachari, A. Rendell, J. C. Burant, S. S. Iyengar, J. Tomasi, M. Cossi, N. Rega, J. M. Millam, M. Klene, J. E. Knox, J. B. Cross, V. Bakken, C. Adamo, J. Jaramillo, R. Gomperts, R. E. Stratmann, O. Yazyev, A. J. Austin, R. Cammi, C. Pomelli, J. W. Ochterski, R. L. Martin, K. Morokuma, V. G. Zakrzewski, G. A. Voth, P. Salvador, J. J. Dannenberg, S. Dapprich, A. D. Daniels, Ö. Farkas, J. B. Foresman, J. V. Ortiz, J. Cioslowski, and D. J. Fox, GAUSSIAN 09, Revision A.1, Gaussian, Inc., Wallingford, CT, 2009.
- <sup>40</sup>J. M. Turney, A. C. Simmonett, R. M. Parrish, E. G. Hohenstein, F. Evangelista, J. T. Fermann, B. J. Mintz, L. A. Burns, J. J. Wilke, M. L. Abrams, N. L. Russ, C. L. Leininger, C. L. Janssen, E. T. Seidl, W. D. Allen, H. F. Schaefer, R. A. King, E. F. Valeev, C. D. Sherrill, and T. D. Crawford, *WIREs: Comput. Mol. Sci.* **2**, 556–565 (2012).